Effect of radio frequency sputtering conditions on the growth and nanomechanical properties of ultrathin amorphous carbon films

W. Lu and K. Komvopoulos
Department of Mechanical Engineering, University of California, Berkeley, California 94720

Abstract

Ultrathin films of amorphous carbon (a-C) were deposited on Si(100) substrates by radio frequency (rf) sputtering using pure Ar as sputtering gas. The films possessed a thickness of 6-95 nm, nanohardness of 12-40 GPa, and root-mean-square (rms) surface roughness of 0.15-32 nm, depending on the deposition conditions. Based on a theoretical analysis for the low-pressure rf Ar discharges in the present system, plasma parameters of the film growth environment were correlated to the deposition conditions to obtain insight into the phenomena responsible for changing the growth characteristics and nanomechanical properties of the a-C films. The surface binding energies of carbon atoms in the films were studied in terms of the measured sputter etching rates resulting from energetic Ar ion bombardment at 850 eV. Higher etching rates were found for a-C films exhibiting higher growth rates and lower hardness. Ultrathin (10 nm) a-C films of maximum hardness (~39 GPa) were synthesized at 3 mTorr working pressure, 750 W rf power, -200 V substrate bias, and 5 min deposition time. Results are presented to elucidate the effects of rf power, working pressure, and substrate bias on the quality of a-C films deposited by controlling the ion-current density, mean free path, and sheath voltages in the rf discharges. The latter are important parameters affecting the ratio of ion and atom fluxes and the intensity (power density) of ion bombardment on the growing film surface.

Submitted to *Journal of Applied Physics* on February 28, 1999.

I. INTRODUCTION

The development of protective ultrathin carbon films exhibiting low friction coefficients, high wear and corrosion resistance, and excellent optical transparency is of great importance to several leading technologies, such as hard disk drives[1] and microelectromechanical devices. Various deposition techniques and characterization methods have been used to study the growth mechanisms and mechanical properties of amorphous carbon (a-C) films free of hydrogen and nitrogen (also referred to as tetrahedral amorphous carbon (ta-C) films due to the high content of sp^3 carbon bonding).[2] Among the different deposition techniques discussed by Lifshitz,[2] such as ion beam, cathodic (vacuum) arc, pulsed laser ablation, ion-assisted evaporation, and sputtering deposition techniques, filtered ion beam and cathodic arc deposition techniques are especially suitable for producing uniform ta-C films. Nevertheless, sputtering deposition of thin a-C films is the most common technique for high-volume production in various industries, such as heads and hard disks for magnetic recording.

Thin a-C films with thickness of several to hundreds nanometers can be deposited using various sputtering techniques.[3-6] In view of recent demands for higher magnetic recording densities, the deposition of hard a-C films of thickness in the range of 5-15 nm has received considerable attention. Although the effects of deposition conditions on the growth and properties of sputtered films have been discussed in previous studies,[2,4,7-10] in particular, the effect of ion bombardment on the growing film surface during magnetron sputtering, comprehensive analyses of the fundamental mechanisms of film growth by sputtering deposition techniques and their effect on the resulting nanomechanical properties of ultrathin (e.g., ~10 nm) carbon films are relatively sparse. Durand *et al.*[11] studied the initial growth of ultrathin carbon films at different substrate temperatures and ion-current densities of carbon ions on the substrate surface and observed that surface roughening commenced upon the transition from lateral to three-dimensional growth. This

transition depended on the effects of the substrate temperature and ion-current density on the film nucleation density and diffusion of carbon material. Anoikin *et al.*[12] studied the scratch resistance of 10-nm-thick protective carbon films and reported a higher scratching resistance for films sputtered at lower substrate temperatures. Puchert *et al.*[13] examined the dependence of intrinsic compressive stresses in carbon films of thickness between 1 and 350 nm sputtered on Si(100) and detected a compressive stress only for continuous films.

The process of thin film deposition by sputtering comprises three main stages: (a) sputtering of film-forming materials from the target surface, (b) transport of sputtered atoms (or clusters of atoms) through the target-substrate space, and (c) adsorption of film-forming precursors and film growth on the substrate surface. Consequently, to study the dependence of the growth and mechanical properties of ultrathin a-C films on the rf sputtering deposition conditions, it is essential to understand the processes of low-pressure rf discharges and the effects of rf power, working pressure, substrate bias voltage, and substrate surface temperature on the aforementioned stages of film deposition.

The rf sputtering technique was used in this study to fabricate ultrathin carbon films using pure Ar as the sputtering gas. The plasma parameters in the film growth environment obtained from an approximate model of the low-pressure rf Ar discharges were used to investigate the effect of deposition conditions on film growth processes. The sputter etching rates of the a-C films due to energetic Ar ion bombardment were used to study the surface binding energies of carbon atoms in films deposited at different conditions. The principal objectives were to investigate the underlying mechanisms of film deposition by rf sputtering and to elucidate the effect of rf power, working pressure, and substrate bias voltage on the plasma parameters affecting the growth characteristics and nanohardness of ultrathin a-C films.

II. EXPERIMENTAL

Ultrathin carbon films were deposited on p-type Si(100) substrates using a commercial rf sputtering system (Perkin-Elmer, Randex-2400 model) without magnetron, shown schematically in Fig. 1. This multi-station sputtering system comprises vacuum, rf power source, gas supply, water cooling, and servo-control systems. Film depositions were performed in a vacuum chamber 70 cm in diameter and 30 cm in height for a target-substrate distance l = 7 cm. The target surface area was equal to that of the substrate holder (i.e., $A_S = A_T$). Pure Ar was used as the sputtering gas at a mass flow rate of 20 sccm. The working pressure was varied between 3 and 10 mTorr by adjusting the opening of a throttle valve in the system; however, in most depositions the chamber pressure was fixed at 3 mTorr. The forwarded rf power was servo-stabilized in the range of 80-1000 W. The reflected rf power was a very small fraction of the forwarded power. Recent x-ray photoelectron spectroscopy studies[14,15] have shown that the carbon films produced under the above sputtering conditions consist of amorphous carbon. The substrate bias was varied between ground potential and -300 V using the substrate tuning technique.[16] Both the target and the substrate holder were maintained at ~20 ^{o}C by water cooling.

The procedure of film deposition involved pumping down first the vacuum chamber to a base pressure less than 5×10^{-6} Torr by a turbo-molecular pump backed by a rotary mechanical pump. After the desired base pressure was reached, a high-purity Ar gas was introduced into the chamber at a mass flow rate of 20 sccm regulated by an MKS® mass flow rate controller. The chamber pressure was then raised to 3, 6, or 10 mTorr by adjusting accordingly the throttle valve. Prior to each film deposition, the graphite target was sputter cleaned for 5-15 min (depending on the previous time of exposure of the chamber) and the Si(100) substrate was sputter etched for 3 min to uniformly remove a 45-nm-thick surface layer. Cleaning of the target and substrate surfaces before film deposition was performed at 250 W rf power and 3 mTorr working pressure.

During the precleaning of the substrate surface, the self-biased substrate voltage was –850 V, whereas the self-biased target voltage during target cleaning was –950 V. The deposition time in most experiments was between 5 and 20 min.

Film thickness measurements were obtained with a stylus profilometer (DEKTAK IID) with a nominal resolution of 0.5 nm. Film growth rates were estimated by dividing the measured film thickness by the corresponding deposition time, assuming uniform film growth during the deposition process. The film surface roughness was determined from 1 μm ×1 μm surface area images obtained with an atomic force microscope (AFM) (Digital Instruments, NanoScope II) operated in the contact mode using sharp silicon tips of nominal radius ~10 nm and contact forces of several nanoNewtons, and a surface force apparatus (SFA) (Hysitron Inc.) using a sharp conical diamond tip of radius ~20 nm and contact force of 0.5 μN. The rms roughness of each film was calculated as the average of at least five roughness values obtained from different AFM maps. Nanoindentation experiments were performed with the SFA using peak indentation loads of 20 μN. Details about the calibration procedures of the SFA and the hardness calculation method have been given elsewhere.[15] The hardness and elastic modulus of the sputtered films were determined from the loading and unloading portions of force-depth curves obtained from indentation experiments performed with the SFA using 20-nm-radius pyramidal diamond tips.

The sputter etching rates of a-C films possessing different thickness, nanohardness, and surface roughness sputtered at a working pressure of 3 mTorr were measured after subjecting simultaneously all the films to energetic Ar ion bombardment. This method was used to study the binding strength of carbon atoms in the films based on a relation between the sputtering yield and surface binding energies of the carbon film materials. The sputter etching experiments were performed at rf power of 250 W, working pressure of 3 mTorr, and Ar gas flow rate of 20 sccm. Under these chamber conditions, the film surfaces were subjected to Ar ion bombardment at

kinetic energy of 850 eV. The duration of these experiments was fixed at 3 min. The thickness of the sputter-etched layer was measured with the DEKTAK IID stylus profilometer. The sputter etching rates of the a-C films were calculated by considering the measured thickness of the removed material (on some ultrathin carbon films some substrate material was also etched away after the films were etched through) and the etching rate of the Si(100) substrate surface, which, under identical sputter etching conditions, was found equal to 15 nm/min. The surface roughness of sputter etched a-C films was also measured to determine the effect of sputter etching on the film surface topography.

III. RESULTS AND DISCUSSION

A. Low-pressure rf Ar discharges

The low-pressure Ar discharges in the present rf sputtering system are parallel plate, capacitive, electropositive discharges containing only Ar ions. To obtain low film growth rates and increased energetic ion bombardment that enhances film densification and re-sputtering of weakly bonded atoms during film deposition, non-magnetron rf sputtering is performed at low working pressures (i.e., 3-10 mTorr). In a low-pressure electropositive Ar plasma the volume electron-ion recombination can be neglected, i.e., the ion loss due to neutralization by electrons in the bulk plasma is negligible, the particle-balance and energy-balance equations can be decoupled.[17] The significance of various plasma parameters in the glow discharges, such as electron and ion temperatures T_e and T_i, respectively, plasma density n_0, kinetic energy E_i and current density J_i of ions bombarding the target and substrate surfaces, ion sound velocity u_B (Bohm velocity) and electron Debye length λ_{De}, have been discussed elsewhere.[17,18] The product of the kinetic energy E_i and current density J_i of the ions bombarding the target or substrate surfaces determines the power density on the target and substrate surfaces during film deposition. In low-pressure plasma discharges, the electron temperature T_e greatly exceeds the ion and neutral

temperatures in the bulk plasma T_i and T, respectively. Typically, T_e is in the range of 2–5 eV (plasma temperatures are usually given in equivalent electron-volt units, 1 eV = 11605 K), whereas T_i and T are a few times the room temperature (i.e. ~0.026 eV). [17]

For Ar plasma at working pressure of 3 mTorr and low-energy ions (e.g., $T_i \approx 0.05$ eV), the ion-neutral mean free path λ_i is ~1 cm, the electron-neutral mean free path is ~4 cm, and the mean sheath thickness s_m at the target and substrate surfaces in this capacitive discharge is ~1 cm.[17] According to Child's law, the sheath thickness also depends on the voltage across the sheath; however, for simplicity it is assumed that the time-averaged thicknesses of the sheathes are equal. Thus, the distance between the target and the substrate holder occupied by the plasma is $d = l - 2s_m$. For Ar gas and 3 mTorr working pressure, the neutral-neutral mean free path λ is ~1.4 cm,[19] and the Knudsen number K_n ($K_n = D/\lambda$, where D is a characteristic dimension of the chamber) is in the range $1 < K_n < 100$, i.e., the gas flow is in the intermediate flow regime,[20] in which the plasma transport is diffusive and the plasma sheathes can be considered to be collisionless.

In the rf discharges for sputtering film deposition, both sheath voltages on the target and the substrate are significantly greater than $T_e/2e$, especially in the presence of a substrate bias voltage, where $T_e/2$ is the directed energy per ion moving at the ion sound velocity u_B (or Bohm velocity) defined as $u_B = (T_e/M_i)^{1/2}$, where M_i is the ion mass. (For $T_e \approx 3.5$ eV and Ar plasma, $u_B \approx 2.9 \times 10^3$ m/s.). Hence, the plasma discharge in the present sputtering system can be approximated by uniform cylindrical plasma of radius r and length d oscillating between the target and substrate surfaces with negligible radial losses. For 3-mTorr rf discharges, the electron Debye length λ_{De}, defined as the scaling distance over which significant charge densities can spontaneously exist, $\lambda_{De} \approx 743(T_e/n_e)^{1/2}$, where T_e is given in eV and the electron density n_e is

given in cm^{-3}, is much smaller than λ_i ($\lambda_{De} << \lambda_i$). For example, for T_e = 3.5 eV and $n_e = 10^{10}$ cm^{-3}, $\lambda_{De} \approx 0.014$ cm $\approx \lambda_i /71$. For this situation, the ion velocity at the plasma-sheath edge u_s is equal to u_B.[17] For uniform plasma density n_0 and collisionless sheaths, the ion-current densities, $J_i = e n_s u_B$, at the target and substrate surfaces are equal. For low-pressure discharges, the ion density at the plasma-sheath edges n_s can be related to the bulk plasma density n_0 by[18]

$$h_l \equiv \frac{n_s}{n_0} \approx 0.86(3 + \frac{l}{2\lambda_i})^{-1/2} . \qquad (1)$$

Considering the particle balance for steady-state low-pressure discharges, the total surface particle loss is equal to the total volume ionization, i.e.,

$$n_s u_B \cdot 2\pi r^2 = n_0 u_B (2\pi r^2 h_l) = K_{iz} n_0 n_g \pi r^2 d , \qquad (2)$$

where K_{iz} is the ionization rate given in cm^3/s and n_g is the neutral gas density given by $n_g = pN_A / RT$, where p is the working pressure, N_A is the Avogadro number, and R is the gas constant, i.e., $n_g \sim 10^{14}$ cm^{-3} for 3 mTorr. Since in a discharge K_{iz} and u_B depend on the electron temperature T_e,[17] Eq. (2) can be written as

$$\frac{K_{iz}(T_e)}{u_B(T_e)} = \frac{1}{n_g d_{eff}} , \qquad (3)$$

where d_{eff} $(= d/(2h_l))$ is an effective discharge length. For 3-mTorr discharges, $d = l - 2s_m \approx 5$ cm and $h_l \sim 0.37$; thus, $d_{eff} \sim 6.76$ cm and $n_g d_{eff} \sim 6.76 \times 10^{14}$ cm^{-2}. Based on the dependence of T_e on $n_g d_{eff}$ for low-pressure Ar plasmas,[17] the estimated electron temperature in the 3-mTorr Ar discharges is ~3.5 eV. Similarly, for 6- and 10-mTorr Ar discharges the corresponding electron temperature is about 2.9 and 2.6 eV, respectively. For low-pressure discharges, it has been suggested that the electron temperature T_e can be determined by particle conservation alone, and is independent of the plasma density and, hence, the absorbed rf power by the discharges.[17]

The discharge power balance for the approximately cylindrical plasma yields, $P_{abs} = n_s u_B A E_T$, where P_{abs} is the power absorbed by the plasma, A is the total surface area for particle loss (including the target and substrate surface areas), and E_T is the total energy lost per ion lost from the plasma system given by $E_T = E_c + E_e + E_i$, where E_c is the collisional energy lost per electron-ion pair created and depends only on T_e for Ar discharges (for T_e = 3.5 eV, $E_c \approx$ 40 eV),[4] E_e is the mean kinetic energy lost per electron lost ($E_e = 2T_e$ for Maxwellian electrons), and E_i is the mean kinetic energy lost per ion lost to the substrate or target surfaces (i.e. the kinetic energy of bombarding ions). Since the directed kinetic energy of Ar ions entering the sheath is equal to ~$T_e/2$, the kinetic energy of each Ar ion impinging on the target surface is approximately equal to the dc potential of the collisionless plasma sheath, i.e., $E_i \approx e(V_0 - V_T) \approx 0.83eV_1$,[17] where V_0 is the bulk plasma potential (typically ~10 V), V_T is the self-biased target voltage that can be measured directly, and V_1 is the fundamental rf voltage amplitude across the sheath. Hence, the power balance equation can be written as

$$P_{abs} = n_s u_B A_T (2E_c + 4T_e + 20 - eV_T - eV_S) = n_s u_B A_T (E' - eV_T - eV_S)$$

(4a)

or

$$S_{abs} = \frac{P_{abs}}{A_T} = n_s u_B (2E_c + 2E_e + 0.83eV_1 - eV_S + 10), \qquad (4b)$$

where V_S is the substrate bias voltage. For 3-mTorr Ar discharges, $E_c \approx$ 40 eV and $E_e \approx$ 7 eV.[17] In the present rf sputtering system, the target is the driven electrode (maintained at a high dc voltage by a blocking capacitor) and the substrate is either grounded or connected to a tuning circuit in order to apply a bias voltage up to –300 V. Therefore, the time-averaged sheath voltages in the rf discharges generated in the sputtering system are asymmetric. The measured target voltage ranges

from –500 to –2100 V, and the substrate bias voltage varies between zero and –300 V. Based on power balance considerations, the sheathes may be considered to be approximately a unified plasma sheath with a total ion loss rate of $n_s u_B A_T$. This assumption will be used later to predict the target voltage based on the energy balance principle for symmetric rf discharges discussed elsewhere.[17] In view of Eq. (4), the directly measured target and substrate bias voltages V_T and V_S, respectively, yield information about the plasma density n_0 and the ion-current density J_i for different deposition conditions.

To develop a comprehensive model for low-pressure rf discharges that can yield estimates of the target bias voltage in terms of the absorbed rf power, it is necessary to consider how the energy is transferred to electrons and indirectly to ions from an external energy source. Electron heating couples most efficiently electric power into the low-pressure rf discharges.[17,18] In this study, the principal electron heating mechanisms are ohmic and stochastic heating, with the latter mechanism prevailing in low-pressure discharges. In ohmic heating, the energy gained from the acceleration of electrons in the bulk plasma electric fields is transferred to thermal electron energy through collisional momentum transfer processes of oscillating electrons and neutrals. Since in low-pressure discharges the collision frequency is low, ohmic heating is not a dominant mechanism in common rf sputtering discharges.

Since the low-pressure rf Ar discharges satisfy condition $\lambda_i \geq (T_i/T_e)d$, the time-averaged power density produced by ohmic heating in the bulk plasma $\overline{S}_{ohm}$ is approximately given by[17]

$$\overline{S}_{ohm} \approx 1.73(\frac{m}{2e})(\frac{n_s}{n_0})\epsilon_0 \omega^2 \nu_m T_e^{1/2} V_1^{1/2} d \ , \qquad (5)$$

where m and e are the mass and charge of an electron, respectively, ϵ_0 is the free-space permeativity, ω is the radian frequency, and ν_m is the electron-neutral collision frequency, i.e., $\nu_m \sim 10^7$ s^{-1} for 3-mTorr Ar discharges.[17]

In stochastic heating, electrons impinging on the oscillating sheath edge change their velocities upon reflection back into the bulk plasma by the sheath-edge movement. As the sheath edge moves toward the bulk plasma, the reflected electrons gain energy, whereas when the sheath edge moves toward the target and substrate surfaces the electrons lose energy. However, the electrons obtain a net energy gain over an oscillation period.[17] For the discharges of this study, the power density due to stochastic heating $\bar{S}_{stoc}$ for a single sheath is approximately given by[17]

$$\bar{S}_{stoc} \approx 0.45(\frac{m}{e})^{1/2} \epsilon_0 \omega^2 T_e^{1/2} V_1 . \tag{6}$$

Hence, for the steady-state low-pressure discharges and unified plasma sheath for ion loss, energy balance between electron heating and electron energy loss due to the loss of electrons yields an equation for the electron power density balance,

$$\bar{S}_{ohm} + 2\bar{S}_{stoc} = n_s u_B (E_e + E_c) , \tag{7}$$

where the sum of E_c and E_e represents the total energy loss per electron lost. Thus, using Eqs. (4) and (7), the target bias voltage ca be related to the absorbed rf power P_{abs} and substrate bias voltage V_S as

$$\frac{S_{abs}}{\bar{S}_{ohm}(V_1) + 2\bar{S}_{stoc}(V_1)} = 2 + \frac{e(0.83V_1 - V_S + 10)}{E_c + E_e} . \tag{8}$$

Hence, using Eqs. (5), (6), and (8), the rf voltage amplitude V_1 can be obtained in terms of the measured absorbed rf power and substrate bias. Then, the target voltage can be obtained as $V_T = -(0.83V_1 - 10)$.

Figure 2 shows a comparison between measured (discrete points) and estimated (lines) target voltages generated in 3-mTorr Ar discharges. The analytical results were obtained from the measured absorbed power and substrate bias voltage at different deposition conditions. While a good agreement between measured and estimated target voltages is obtained at a substrate bias of –100 V, at ground potential and –200 V the analytical predictions underestimate and

overestimate, respectively, the actual values of the target voltage. For fixed chamber geometry, absorbed power, working pressure, and substrate bias, Eq. (4) indicates that an underestimated target voltage corresponds to an overestimated plasma density. However, Fig. 3 shows that for 6- and 10-mTorr Ar discharges and zero substrate bias voltage the model underestimates the plasma density. This is because at 6 and 10 mTorr the mean free path for all kinds of collisions in the discharges is about one half and one third, respectively, that at 3 mTorr. Hence, while the assumption of collisionless sheaths is reasonable for the 3-mTorr discharges, it induces some error in the predictions of the target bias voltage at 6 and 10 mTorr. Despite this disagreement, it will be shown later that the low-pressure discharge model provides useful insight into the dependence of growth rate and properties of the a-C films on the rf sputtering deposition conditions.

Figure 4 shows the dependence of the ion-current density on the absorbed rf power at 3 mTorr. The discrete data points represent the ion-current density obtained from the measured absorbed power and substrate bias voltage ranging from ground potential to –300 V. The results indicate that at 3 mTorr the ion-current density varies with the square root of the absorbed rf power, i.e., $J_i \propto P_{abs}^{1/2}$. Since the substrate bias is applied by a substrate tuning technique,[16] applying a substrate bias changes the power density ($E_i J_i/e$) distribution between the target and the substrate, although it does not change the ion-current density appreciably. This indicates that the ion-current density and ion bombarding energy to the substrate surface during film deposition can be independently controlled in the present sputtering system.

B. Carbon film deposition without substrate bias

In sputtering deposition of a-C films, carbon atoms (or clusters of atoms) sputtered from the target are mostly neutral and their kinetic energy ranges from several eV to tens eV,[17,19] depending on the mass and kinetic energy of incident ions. Particles bombarding on the growing film surface at such kinetic energy levels rarely cause re-sputtering of carbon material from the

film surface. However, film-forming carbon atoms with kinetic energies of tens of eV produced from sputtering of the target surface or from low-energy particle bombardment on the film surface possess a higher mobility on the surface and in the bulk of the growing film, which is beneficial to the film densification and material property enhancement. Since in the absence of substrate bias the kinetic energy of bombarding Ar ions on the growing film surface is about 10 eV, re-sputtering of film material is negligibly small. Therefore, the effects of the rf power and working pressure on the film growth and properties can be elucidated by studying the deposition rate, surface roughness, and nanoindentation hardness of the films deposited without substrate bias.

Figure 5(a) shows that the growth rate of a-C films deposited without substrate bias varies linearly with the absorbed rf power measured during film deposition. Since all the data points shown in the figure were obtained from experiments performed at working pressure of 3 mTorr and mass flow rate of 20 sccm, the scattering effect during the transport of carbon atoms and carbon clusters across the target-substrate space should be the same in all cases. Hence, the film growth rate in the absence of substrate bias reflects the sputtering rate of carbon material from the target surface. Figure 5(b) shows a linear relationship between the power density on the target surface (calculated based on the discharge model discussed previously) and the absorbed rf power. This indicates that the sputtering rate of carbon material from the graphite target surface is proportional to the power density at the target surface.

Figure 6(a) shows the dependence of surface roughness on the film growth rate of the a-C films deposited without substrate bias at a working pressure of 3 mTorr. The results reveal that higher deposition rates without energetic ion bombardment produce rougher films. Increasing the flux of incoming carbon atoms decreases the time and likelihood of newly adsorbed carbon atoms to migrate to lower-potential sites. In view of the reduced mobility of adsorbed carbon atoms, higher deposition rates without substrate bias yield films with rougher topographies and lower

densities. In the absence of substrate biasing, the growth rate effect on the film density is reflected in the resulting film hardness. As shown in Fig. 6(b), significantly softer a-C films were produced at higher growth rates and working pressure of 3 mTorr without substrate biasing.

Results showing the effect of working pressure on the film deposition rate (thickness) and nanohardness of some a-C films deposited at different working pressure and without substrate biasing are given in Table I. A comparison of the data shows that the thickness and nanohardness of the a-C films increase significantly with decreasing working pressure, for similar power density on the target surface and deposition time. Since the sputtering rate of carbon material is proportional to the power density at the target surface, shown in Fig. 5(b), the results shown in Table I can be interpreted in terms of the enhancement of the scattering effect by collisions during the transport of carbon atoms through the target-substrate space, resulting from the decrease of the mean free path in the discharge at higher working pressures. Furthermore, the higher collision frequency encountered by the carbon particles during transport increases the loss of kinetic energy of film-forming precursors, i.e., at higher working pressure the amount and kinetic energy of film-forming precursors deposited on the substrate surface decrease simultaneously. Therefore, the working pressure affects mainly the scattering and kinetic energy loss of the precursors traveling across the target-substrate space due to changes of the mean free path in the plasma discharge. Consequently, for carbon film deposition by rf sputtering without substrate biasing, both the film growth rate and the kinetic energy of film-forming precursors control the film hardness. Therefore, lower deposition rates and higher kinetic energies of film precursors are beneficial to the film nanohardness.

C. Sputter etching of carbon films

The sputter etching rate in noble gas discharges is equivalent to the sputtering yield ***g***, defined as the number of atoms ejected from the bombarded surface per incident ion. The critical

kinetic energy for atom extraction from an ion bombarded surface by an incident energetic ion is typically 1 keV.[19-23] For ion kinetic energies less than 1 keV, the sputtering yield depends on the energy transfer and is given by[23]

$$\boldsymbol{g} = \frac{3\boldsymbol{a}}{4\boldsymbol{p}^2}\frac{4m_i m_t}{(m_i + m_t)}\frac{E_i}{U_0}, \tag{9}$$

where m_i and m_t represent the masses of incident ions and target atoms, respectively, U_0 is the surface binding energy of the sputtered material, and $\boldsymbol{a}$ is a monotonic function of m_t/m_i, increasing from 0.17 to 1.4 as m_t/m_i increases from 0.1 to 10. For ion kinetic energies greater than 1 keV, the input energy is dissipated within a larger volume of target material. Hence, the energy dissipated in the surface layers remains virtually constant over a broad energy range, and the sputtering yield is essentially independent of the bombarding ion energy E_i and target atom density and is approximated as[17, 23]

$$\boldsymbol{g} \propto \frac{m_i}{m_i + m_t}\frac{1}{U_0}. \tag{10}$$

Therefore, the sputter etching rate of the a-C films can be determined by the sputtering yield of the carbon film material subjected to energetic ion bombardment at 850 eV using Eq. (9). Since all the samples were sputter etched under the same conditions, only the surface binding energy U_0 in Eq. (9) differs. Thus, the relative surface binding energy of the different a-C film materials can be determined by comparing the measured etching rates.

Under the same sputter etching conditions, the sputter etching rate of p-type Si(100) was found equal to 15 nm/min. The sputter etching rate of silicon R is given by

$$R = \boldsymbol{g}_{Si}\frac{J_i}{e}\frac{1}{n_{Si}},$$

(11)

where γ_{Si} is the sputtering yield of single crystal due to Ar ion bombardment, n_{Si} is the silicon atom density in the single crystal state, and J_i is the ion-current density estimated based on the aforementioned method. For 600 eV Ar ion bombardment $\gamma_{Si} \approx 0.54$.[19,23] Since the single crystal silicon has a mass density of 2.33 g/cm^3, the corresponding atom density is estimated to ~5 x 10^{28}m^{-3}. In the sputter etching experiments the substrate holder is rotated away from the target and a parallel plate at ground potential is placed opposite to each surface. The application of the same rf power to the target and substrate surfaces produces two discharges. Since the adsorbed power during sputter etching was 248 W (i.e., the reflected power was equal to 2 W), the ion-current density on the etched samples is estimated to be ~3.28 A/m^2. Then, the sputter etching rate of Si(100) obtained from Eq. (11) for $\gamma = 0.54$ is calculated to be ~13.3 nm/min, which is close to the measured value of 15 nm/min. The small difference is due to the underestimated magnitude of the sputtering yield coefficient, since the kinetic energy of bombarding Ar ions was equal to 850 eV.

Figure 7 shows the variation of the sputter etching rate with the growth rate and nanohardness of a-C films deposited at a working pressure of 3 mTorr. The increase of the etching rate with the film growth rate, shown in Fig. 7(a), suggests that a-C films with lower growth rates exhibit a higher surface binding energy. This is because at lower film growth rates the newly adsorbed carbon atoms on the growing film surface have more time to migrate to surface sites of lower potential energy. In addition, substrate biasing intensifies the bombardment of energetic Ar ions, thereby promoting the removal of weakly bonded carbon atoms and the slower growth of films exhibiting higher surface binding energies. Thus, the more pronounced re-sputtering of weakly bonded carbon atoms during film growth yields films possessing higher surface binding energies and increased nanohardness. In view of Fig. 7(b), it may be interpreted

that harder carbon films exhibit higher surface binding energies due to the significantly lower sputter etching rates.

Figure 8 shows the surface roughness of a-C films before and after argon plasma etching versus the film nanohardness. The rms roughness of the sputter etched Si(100) substrate was found equal to 0.22 ± 0.03 nm, i.e., identical to the roughness of the original substrate surface. Films with nanohardness over 30 GPa exhibited significant roughening upon plasma etching, whereas sputter etching smoothed out the topographies of softer films. The relatively rougher a-C films are characterized by higher deposition rates. Although the surface roughness of as-deposited a-C films varies appreciably, after sputter etching for 3 min the films exhibited similar roughness values. This suggests that the a-C films deposited by rf sputtering in the low-pressure regime possessed fairly homogeneous microstructures.

The above sputter etching studies indicate that ultrathin hard a-C films with high surface binding energies can be synthesized at lower working pressures and film growth rates (in the absence of substrate biasing) by promoting energetic ion bombardment in order to remove weak atomic bonds at the growing film surfaces.

D. Carbon film deposition with substrate biasing

Since film deposition depends on the competing processes of arriving atoms sputtered from the graphite target and sputter etching of weakly adsorbed atoms at the film surface, energetic Ar ion bombardment plays a critical role during a-C film growth in rf sputtering. Substrate biasing is therefore beneficial to the quality of the deposited films because it promotes weak bond removal and film densification. Consequently, a-C films with significantly different nanomechanical properties can be produced by biasing the substrate, as shown in the following section. Carbon film growth on Si(100) depends on the arrival and re-sputtering rates of carbon precursors. Hence, the film growth rate depends on the sticking probability of newly adsorbed carbon atoms,

which depends on the material system, substrate temperature, and ion bombardment during film growth. Although, the substrate holder was maintained at 20 ^{o}C by water cooling, relatively high temperatures might have occurred at the growing film surfaces due to the increased intensity of energetic ion bombardment. Durand *et al*.[11] observed that over a critical substrate temperature it is impossible to obtain ultrathin carbon films of high smoothness due to the low nucleation rates accompanied by significant surface migration.

Figure 9 shows the effect of substrate biasing on the deposition and sputter etching rates and the nanohardness of a-C films deposited at a working pressure of 3 mTorr and forwarded rf power of 500 and 750 W. At both powers, the self-biased target voltage during deposition is greater than 1 kV, as shown in Fig. 2. Thus, under the deposition conditions mentioned above, the sputtering rate of carbon material from the target surface depends only on the ion-current density. This is evident from Eq. (10) showing that the sputtering yield in this regime mainly depends on the surface binding energy of the graphite surface. As shown in Fig. 4 for 3-mTorr discharges, the ion-current density depends on the absorbed rf power that is approximately equal to the forwarded power (for a well-tuned rf sputtering system). Therefore, any differences in the growth and properties of the sputtered films are mainly attributed to the processes occurring on the growing film surface (such as ion bombardment and deposition) because the conditions for material sputtering from the target and material transport across the target-substrate space are almost identical. As shown in Fig. 9, substrate biasing decreases the film growth rate due to the re-sputtering of carbon film material by bombarding energetic ions. The decrease of the etching rate accompanied by the increase of the film hardness indicates that substrate biasing affects the film microstructure. The lowest growth and etching rates and highest hardness are obtained for a bias of –200 V. This optimum condition arises because at this bias voltage weak carbon bonds are effectively removed without damaging the film microstructure. At higher bias voltage, e.g., –300

V, ion irradiation damage during film growth is considered to be the main reason for the reduced film density. At such high bombarding kinetic energies, migration of implanted film atoms due to the occurrence of thermal spikes becomes more dominant than the effect of knock-on implantation enhancing film densification during deposition.[24] This is supported by the increase of the deposition and etching rates and the decrease of the film hardness observed upon changing the substrate bias from –200 to –300 V.

The trends shown in Fig. 9 are in good agreement with the findings of Schwan *et al.*[4] for ta-C films fabricated by rf magnetron sputtering at similar power densities. For argon ion-to-neutral carbon flux ratio of ~5, the film density and compressive stress were reported to reach a maximum of 2.7 g/cm^3 and 16 GPa, respectively, at an ion bombarding energy of ~100 eV. Since a residual compressive stress is due to the dilatational strain caused by energetic ion bombardment during film growth, the maximum values of the film density and compressive stress should arise simultaneously under the same film growth conditions. Puchert *et al.*[13] have argued that the average film density influences the macroscopic stress in sputtered carbon films. Rossi *et al.*[25] observed that maximum-density carbon films exhibited optimum mechanical properties. It has been reported that a compressive stress increases the resistance of ultrathin carbon films to plastic deformation.[26,27] Thus, the carbon films possessing the highest density and compressive stress are expected to also exhibit the highest hardness.

Since the kinetic energy of Ar ions bombarding the target surface is greater than 1 keV for both 500 and 750 W, the sputtering yield of carbon material by argon ions in this study is equal to ~0.2.[23] Thus, the argon ion-to-neutral carbon atom flux ratio during sputtering deposition of the a-C films is ~5. From Fig. 4, the ion-current density J_i for 750-W rf power is ~1 mA/cm^2. Therefore, at substrate bias of –200 V and rf power of 750 W, the power density (E_iJ_i/e) at the growing film surface is ~0.2 W/cm^2. In the rf magnetron sputtering system of Schwan *et al.*,[4] the

estimated ion-current density is ~2 mA/cm^2, based on the same deposition conditions given elsewhere,[28] i.e., the maximum compressive stress was also found to occur at a power density at the growing film surface of 0.2 W/cm^2. This interesting finding suggests that the power density at the growing film surface is a critical parameter controlling the growth rate and mechanical properties of the a-C films. Fallon *et al.*[29] studied the effect of ion energy on the properties of ion-beam diamondlike carbon films and reported that the optimum kinetic energy of film-forming carbon ions depends on the type and, probably, deposition flux rate of carbon ions.

A high power density at the film surface may raise the surface temperature appreciably, thereby enhancing the surface diffusion of adsorbed carbon atoms, especially if the thermal energy due to surface heating is above the activation energy threshold for carbon surface diffusion. In the present experiments, the substrate temperature was maintained low to minimize surface diffusion of adatoms, that is responsible for surface roughening and the degradation of the film nanomechaical properties. Figure 10 shows the dependence of the rms surface roughness of a-C films on the ion-current density J_i and substrate bias voltage V_S. Based on Fig. 10, the threshold of the power density is estimated to be ~0.25 W/cm^2. For rf power of 950W and substrate bias of –200 and –300 V, the film surface roughness increases significantly. In fact, the rms roughness values are greater than the film thickness. The 20-nm thick carbon film deposited at a substrate bias of –200 V has an rms roughness of 26.4 nm, whereas the rms roughness of the 17-nm thick carbon film deposited at substrate bias of –300 V is ~32 nm. The high surface roughness values are attributed to surface heating due to the high power density at the growing film surface that might have promoted the migration of newly adsorbed carbon atoms toward previously formed islands of carbon material by surface diffusion. Lifshitz *et al.*[30] reported a critical temperature of 150 ^{o}C for surface diffusion to occur on diamondlike carbon films deposited on Si(100) at a mean kinetic energy of 120 eV. Sattel *et al.*[31] reported that the surface roughness and mechanical and

optical properties of hydrogenated ta-C films changed at a critical substrate temperature (depending on the ion energy) because of the thermally activated migration of subplanted carbon atoms. Due to carbon clustering at high temperatures, exposed areas of the substrate surface are subjected to energetic ion bombardment during the film growth process resulting in the selective removal of silicon from the substrate surface. Alternatively, at surface areas where carbon was deposited, film deposition continues to occur at a rate exceeding the removal rate of carbon material due to energetic ion bombardment. These conditions yield rough topographies characterized by the partial coverage by carbon material.

E. Nanomechanical properties of amorphous carbon films

The ratio of the material hardness to the in-plane elastic modulus $H(1-\mathbf{n}^2)/E$ is a plasticity parameter characterizing the resistance to plastic deformation. Figure 11 shows that the ratio $H(1-\mathbf{n}^2)/E$ increases monotonically with the nanohardness H of the sputtered a-C films. It has been suggested that the irreversible-to-total work ratio for a complete load-unload indentation cycle is proportional to the hardness-to-elastic modulus ratio.[32] This is in qualitative agreement with the trend shown in Fig. 11.

As discussed in the previous section, substrate biasing affects significantly the energetic ion bombardment and re-sputtering processes occurring at the growing film surface. This may have profound implications on the nanomechanical behavior of the deposited films. An illustrative example of this effect is shown in Fig. 12. The results were obtained from nanoindentations performed on 10-nm-thick a-C films with growth rates fixed at 2 nm/min. The indentation force-displacement curves reveal a strong effect of the rf power and substrate bias voltage on the mechanical behavior of the films. The nanohardness and in-plane elastic modulus of the a-C film deposited at rf power of 250 W without substrate biasing are 17.3 ± 0.9 GPa and 124.9 ± 5.7 GPa, respectively. The large force hysteresis is indicative of the development of relatively

significant plastic deformation in the film [curve (b)]. However, the hardness and elastic modulus of the film deposited at 750 W rf power and substrate bias of –200 V are 39.2 ± 3.5 GPa and 185.1 ± 9 GPa, respectively, and the film exhibits virtually purely elastic behavior [curve (a)].

The effect of substrate biasing on the elastic-plastic properties of ultrathin a-C films deposited at rf power of 750 W and chamber pressure of 3 mTorr is shown in Fig. 13. The remarkable differences between the loading and unloading portions of the indentation cycles indicate a profound effect of substrate biasing on the resulting film microstructure. The force hysteresis area of each indentation curve indicates the amount of irreversible work in each film. A comparison of the indentation curves shown in Fig. 13 shows that a-C films with maximum elastic stiffness and penetration resistance were synthesized at a substrate bias voltage of –200 V [Fig. 13(c)]. The very small contact force (~1 μN) detected after retracting the diamond tip back to its original position is most likely due to contact with the upwardly bulged film resulting from the relaxation of residual compressive stress. Results for the nanomechanical properties and elastic-to-total work ratio W_{el}/W_{tot} of a-C films, obtained from the indentation force-displacement curves shown in Fig. 11 following the methods presented in a previous study,[15] are listed in Table II in terms of the film thickness and substrate bias voltage. It is noted that H, $H(1-\nu^2)/E$, and W_{el}/W_{tot} vary with the substrate bias in a similar fashion. For the 20-μN peak load used in the nanoindentation experiments, the 10-nm-thick a-C films deposited at substrate bias of –200 V exhibit the higher hardness-to-elastic modulus ratio (0.212) and virtually zero plastic deformation (W_{el}/W_{tot} = 1.0). It is apparent that the elastic recovery increases with the hardness-to-elastic modulus ratio. A recent study on the nanotribological properties of a-C films has revealed that substrate biasing at –200 V produces a-C films with maximum wear resistance.[33] Although the films obtained at zero and –300 V bias voltage exhibit very similar mechanical behaviors (samples A and D in Table II), the corresponding indentation force-displacement curves [Figs. 13(a) and 13(d)] are not identical. An

examination of the diamond tip after indentation testing, however, revealed small changes in the tip shape. The results shown in Fig. 13 were obtained with two different tip shape functions; one for samples A and C and another one for samples B and D. As shown in Fig. 14, the variations of the two tip shape functions (represented by the projected area of indentation) with the contact depth are slightly different, presumably due to mild deformation of the tip. However, Figs. 13(a) and 13(d) and Table II show that the films exhibit identical elastic recovery. This is expected since the elastic material response is insensitive to the tip shape.

In summary, the presented results indicate that ultrathin a-C films with optimum nanomechanical properties can be fabricated by rf sputtering, provided the plasma parameters in the Ar discharges are controlled to yield optimum deposition conditions.

IV. CONCLUSIONS

Based on an approximate model for low-pressure Ar discharges in rf sputtering, the plasma parameters were correlated to the deposition conditions of ultrathin a-C films. Specifically, the effects of rf power, working pressure, and substrate bias voltage on the growth characteristics and nanohardness of a-C films were studied in light of experimental and analytical results. Based on the presented results and discussion, the following main conclusions can be drawn.

(1) Results for the plasma parameters derived from an approximate model for low-pressure rf discharges are in good agreement with measured values, especially for 3-mTorr working pressure.

(2) In 3-mTorr Ar rf discharges, the absorbed power determines the ion-current density at the target and substrate surfaces, i.e., the ion-current density and ion bombarding energy at the substrate surface can be independently controlled in the present rf sputtering system.

(3) The working pressure determines the mean free path of charged and neutral particles in the discharges, and, thus, affects the scattering and kinetic energy loss of film forming carbon precursors.

(4) Energetic Ar ion bombardment on the growing film surface affects significantly the quality of the deposited a-C films. Substrate biasing increases the kinetic energy of bombarding ions; however, its effectiveness depends mainly on the power density at the substrate surface, which is the product of the ion bombarding kinetic energy and the ion-current density.

(5) High kinetic energies of the ions bombarding on the growing film surface degrade the film quality. Intensive ion bombardment on the film surface may increase the surface temperature sufficiently to promote surface diffusion leading to the formation of discontinuous films.

(6) The measured sputter etching rate provides insight into the interdependence of the growth rate, surface binding energy, and nanohardness of a-C films.

(7) Radio frequency Ar discharges at working pressure of 3 mTorr, rf power of 750 W, substrate bias of –200 V, and deposition times of ~5 min produce 10-nm-thick a-C films of low rms roughness (~0.2 nm), maximum hardness (~39.19 GPa), and high hardness-to-elastic modulus ratio (0.212).

ACKNOWLEDGMENTS

This research was supported by the Surface Engineering and Tribology Program of the National Science Foundation under Grant No. CMS-9734907 and the Computer Mechanics Laboratory at the University of California at Berkeley.

References

[1]H. Tsai and D. B. Bogy, J. Vac. Sci. Technol. A **5**, 3287 (1987).

[2]Y. Lifshitz, in *The Physics of Diamond*, edited by A. Paoletti and A. Tucciarone (IOS, Amsterdam, 1997), pp. 209-253.

[3]S. Logothetidis and G. Stergioudis, Appl. Phys. Lett. **71**, 2463 (1997).

[4]J. Schwan, S. Ulrich, H. Roth, H. Ehrhardt, S. R. P. Silva, J. Robertson, R. Samlemski and R. Brenn, J. Appl. Phys. **79**, 1416 (1996).

[5]J. J. Cuomo, D. L. Pappas, J. Bruley, J. P. Doyle and K. L. Saebger, J. Appl. Phys. **70**, 1706 (1991).

[6]D. L. Pappas, K. L. Saenger, J. Bruley, W. Krakow, J. J. Cuomo, T. Gu and R. W. Collins, J. Appl. Phys. **71**, 5675 (1991).

[7]J. Schwan, S. Ulrich, T. Theel, H. Roth, H. Ehrhardt, P. Becker and S. R. P. Silva, J. Appl. Phys. **82**, 6024 (1997).

[8]S. Seo, D. C. Ingram and H. H. Richardson, J. Vac. Sci. Technol. A **13**, 2856 (1995).

[9]A. Lousa and S. Gimeno, J. Vac. Sci. Technol. A **15**, 62 (1997).

[10]O. Auciello and R. Kelly, *Ion Bombardment Modification of Surfaces* (Elsevier, Amsterdam, 1984).

[11]H. A. Durand, K. Sekine, K. Etoh, K. Ito and I. Kataoka, J. Appl. Phys. **84**, 2591 (1998).

[12]E. V. Anoikin, M. M. Yang, J. L. Chao, J. R. Elings and D. W. Brown, J. Vac. Sci. Technol. A **16**, 1741 (1998).

[13]M. K. Puchert, P. Y. Timbrell, R. N. Lamb and D. R. McKenzie, J. Vac. Sci. Technol. A **12**, 727 (1994).

[14]W. Lu and K. Komvopoulos, J. Appl. Phys. (1999) (submitted).

[15]W. Lu and K. Komvopoulos, J. Appl. Phys. **85**, 2642 (1999).

[16]J. S. Logan, IBM J. Res. Develop. **14**, 172 (1970).

[17]M. A. Lieberman and A. J. Lichtenberg, *Principles of Plasma Discharges and Materials Processing* (Wiley, New York, 1994).

[18]M. A. Lieberman, G. S. Selwyn and M. Tuszewski, MRS Bull. **21**(8), 32 (1996).

[19]M. Konuma, *Film Deposition by Plasma Techniques* (Springer, Berlin, 1992).

[20]M. Ohring, *The Material Science of Thin Films* (Academic, Boston, 1992).

[21]J. E. Mahan and A. Vantomme, J. Vac. Sci. and Technol. A **15**, 1976 (1997).

[22]P. Sigmund, Phys. Rev. **184**, 383 (1969).

[23]B. Chapman, *Glow Discharge Processes* (Wiley, New York, 1980).

[24]C. A. Davis, Thin Solid Films **226**, 30 (1993).

[25]F. Rossi, B. Andre, A. van Veen, P. E. Mijnarends, H. Schut, F. Labohm, H. Dunlop, M. P. Delplancke and K. Hubbard, J. Mater. Res. **9**, 2440 (1994).

[26]K. Komvopoulos, N. Ye and W. Lu, unpublished work.

[27]S. Umemura, Y. Andoh, S. Hirono, T. Miyamoto and R. Kaneko, Phil. Mag. A **74**, 1143 (1996).

[28]S. Ulrich, J. Scherer, J. Schwan, I. Barzen, K. Jung, M. Scheib and H. Ehrhardt, Appl. Phys. Lett. **68**, 909 (1996).

[29]P. J. Fallon, V. S. Veerasamy, C. A. Davis, J. Robertson, G. A. J. Amaratungs, W. I. Milne and J. Koskinen, Phys. Rev. B **48**, 4777 (1993).

[30]Y. Lifshitz, G. D. Lempert and E. Grossman, Phys. Rev. Lett. **72**, 2753 (1994).

[31]S. Sattel, J. Robertson and H. Ehrhardt, J. Appl. Phys. **82**, 4566 (1997).

[32]Y.-T. Cheng and C.-M. Cheng, Appl. Phys. Lett. **73**, 614 (1998).

[33]W. Lu and K. Komvopoulos, J. Tribol. (1999) (submitted).

Table I. Thickness and nanohardness of a-C films vs. sputtering deposition conditions.[a)]

Working pressure (mTorr)	Forward power (W)	Absorbed power (W)	Power density on target (W/cm^2)	Deposition time (min)	Film thickness (nm)	Film nanohardness (GPa)
3	200	190	0.48	20	52.6	25.4±1.9
3	200	190	0.48	40	95	24.4±2.5
6	200	185	0.47	20	24	21.3±1.7
6	200	185	0.47	40	59	17.7±1.7
3	250	237	0.61	10	20	20.4±1.7
3	250	240	0.62	15	31	19.4±0.6
10	250	230	0.59	10	10	14.6±1.0
10	250	240	0.62	15	21	11.4±1.3

[a)] No substrate biasing.

Table II. Nanomechanical properties of rf sputtered a-C films.[a)]

Sample	Bias (V)	Thickness (nm)	rms (nm)	H (GPa)	$E/(1-\mathbf{n}^2)$ (GPa)	$\frac{H(1-\mathbf{n}^2)}{E}$	$\frac{W_{el}}{W_{tot}}$
A	0	27	0.90 ±0.06	19.67 ±1.41	132.61 ±4.36	0.148	0.57
B	-100	22	0.18 ±0.02	34.20 ±0.72	197.69 ±13.19	0.173	0.70
C	-200	10	0.20 ±0.05	39.19 ±3.53	185.10 ±9.00	0.212	1.00
D	-300	17	0.19 ±0.08	19.84 ±1.22	133.19 ±6.06	0.149	0.52

[a)]rf power = 750 W; working pressure = 3 mTorr; deposition time = 5 min.

List of Figures

FIG. 1 Schematic diagram of the rf sputtering system.

FIG. 2 Measured (symbols) and estimated (lines) target bias voltages vs absorbed rf power and substrate bias voltage for working pressure equal to 3 mTorr.

FIG. 3 Measured (symbols) and estimated (lines) target bias voltages vs absorbed rf power for zero bias voltage and working pressure equal to 6 and 10 mTorr.

FIG. 4 Ion-current density vs absorbed rf power for working pressure equal to 3 mTorr and substrate bias between zero and –300 V.

FIG. 5 Variation of (a) film growth rate and (b) power density at target surface on absorbed rf power for zero substrate bias and working pressure equal to 3 mTorr.

FIG. 6 Variation of (a) rms roughness and (b) nanohardness of a-C films with film growth rate for zero substrate bias.

FIG. 7 Variation of sputter etching rate of a-C films with (a) film growth rate and (b) nanohardness for working pressure equal to 3 mTorr and substrate bias between zero and –300 V.

FIG. 8 Surface roughness vs nanohardness of a-C films before and after Ar ion bombardment at 850 eV.

FIG. 9 Variation of (a) deposition rate, (b) sputter etching rate, and (c) nanohardness of a-C films with substrate bias voltage for forwarded rf power equal to 500 and 750 W.

FIG. 10 Dependence of surface roughness of a-C films on ion-current density and substrate bias voltage during sputtering deposition for working pressure equal to 3 mTorr.

FIG. 11 Hardness-to-elastic modulus ratio vs nanohardness of a-C films.

FIG. 12 Contact force vs displacement curves of indented a-C films for 2 nm/min deposition rate and 3 mTorr working pressure: (a) 750 W rf power and –200 V bias voltage, and (b) 250 W rf power and zero bias voltage.

FIG. 13 Contact force vs displacement curves of indented a-C films for substrate bias voltage equal to (a) 0 V (sample A), (b) –100 V (sample B), (c) –200 V (sample C), and (d) –300 V (sample D). (rf power = 750 W; working pressure = 3 mTorr; and deposition time = 5 min).

FIG. 14 Tip shape functions for samples A-D.

Figure 1:

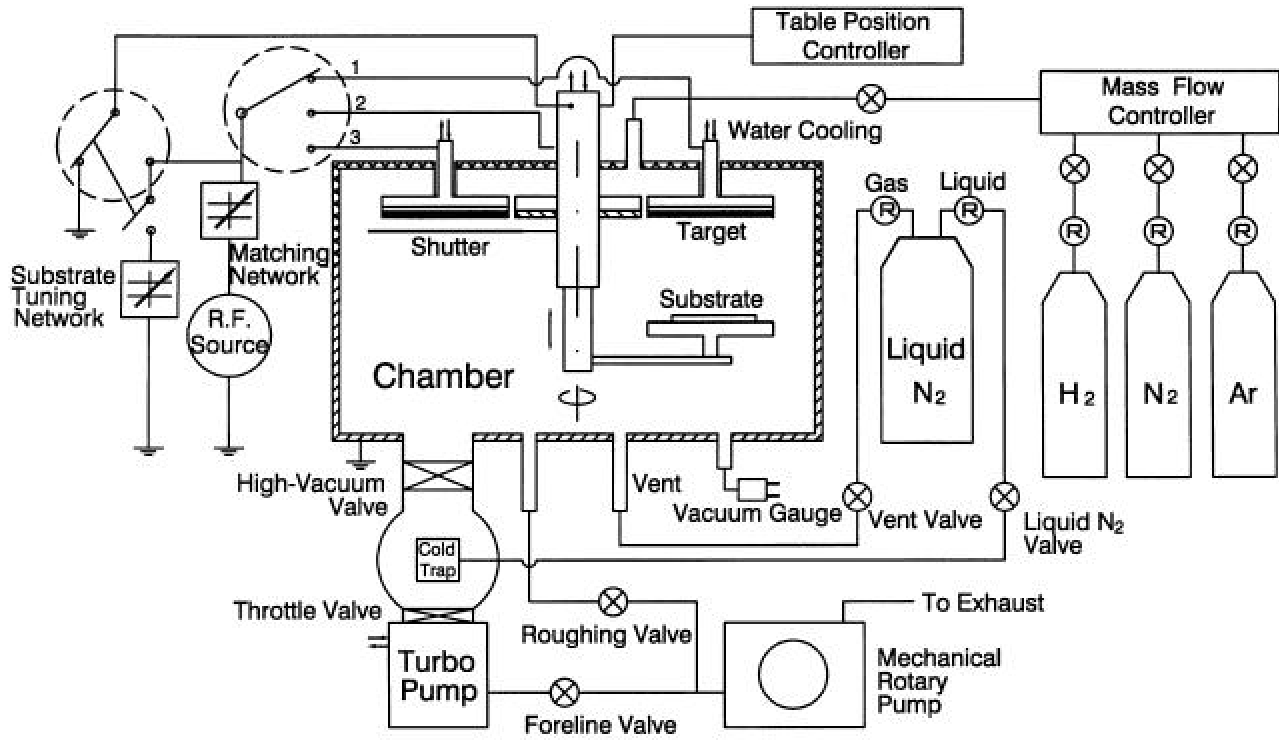

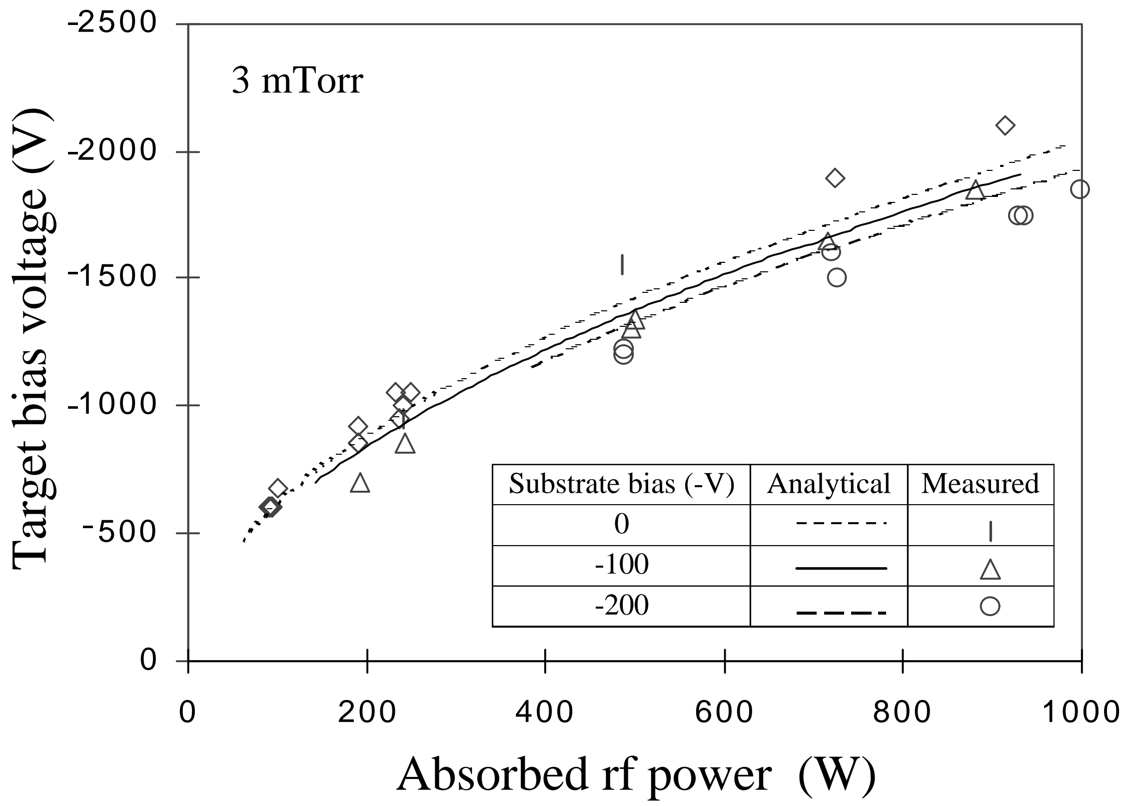

Figure 2

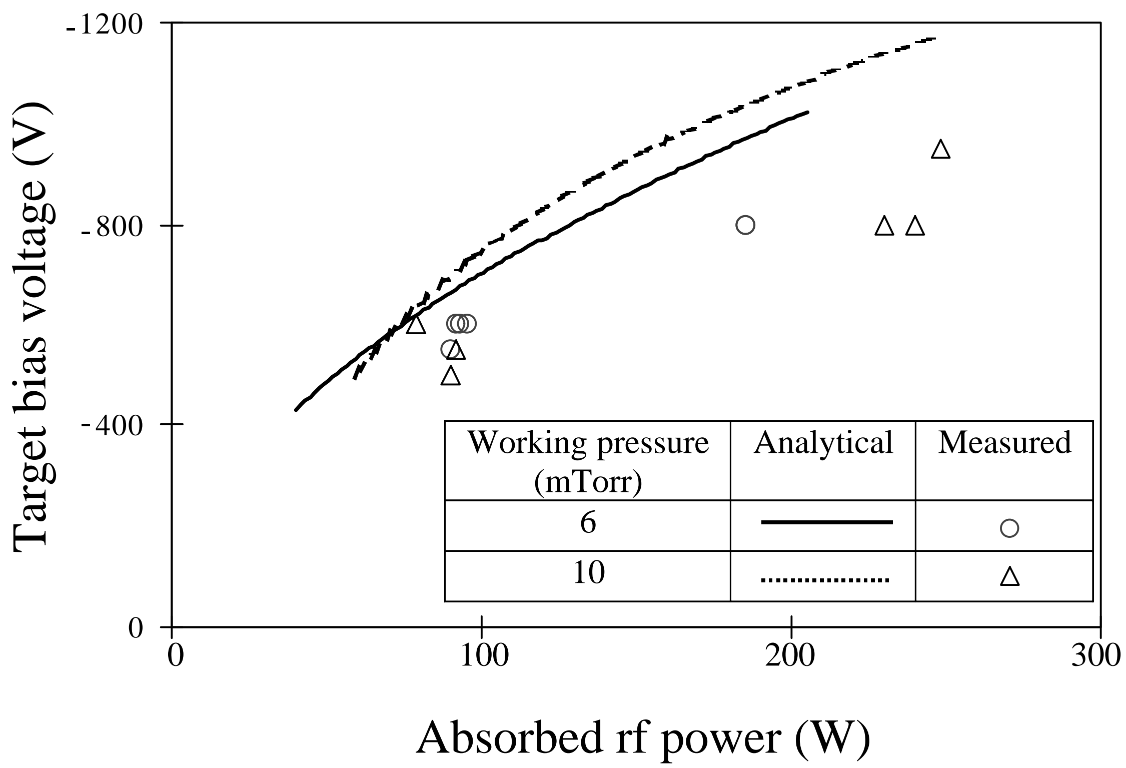

Figure 3

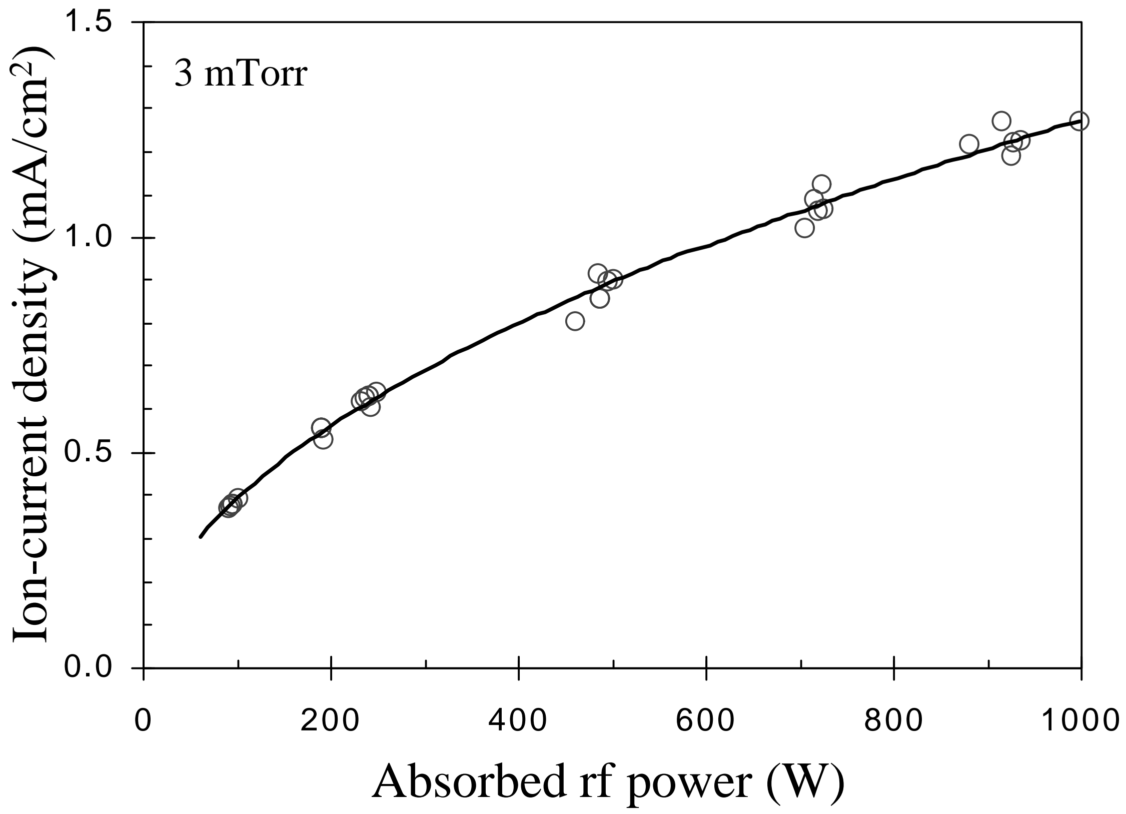

Figure 4

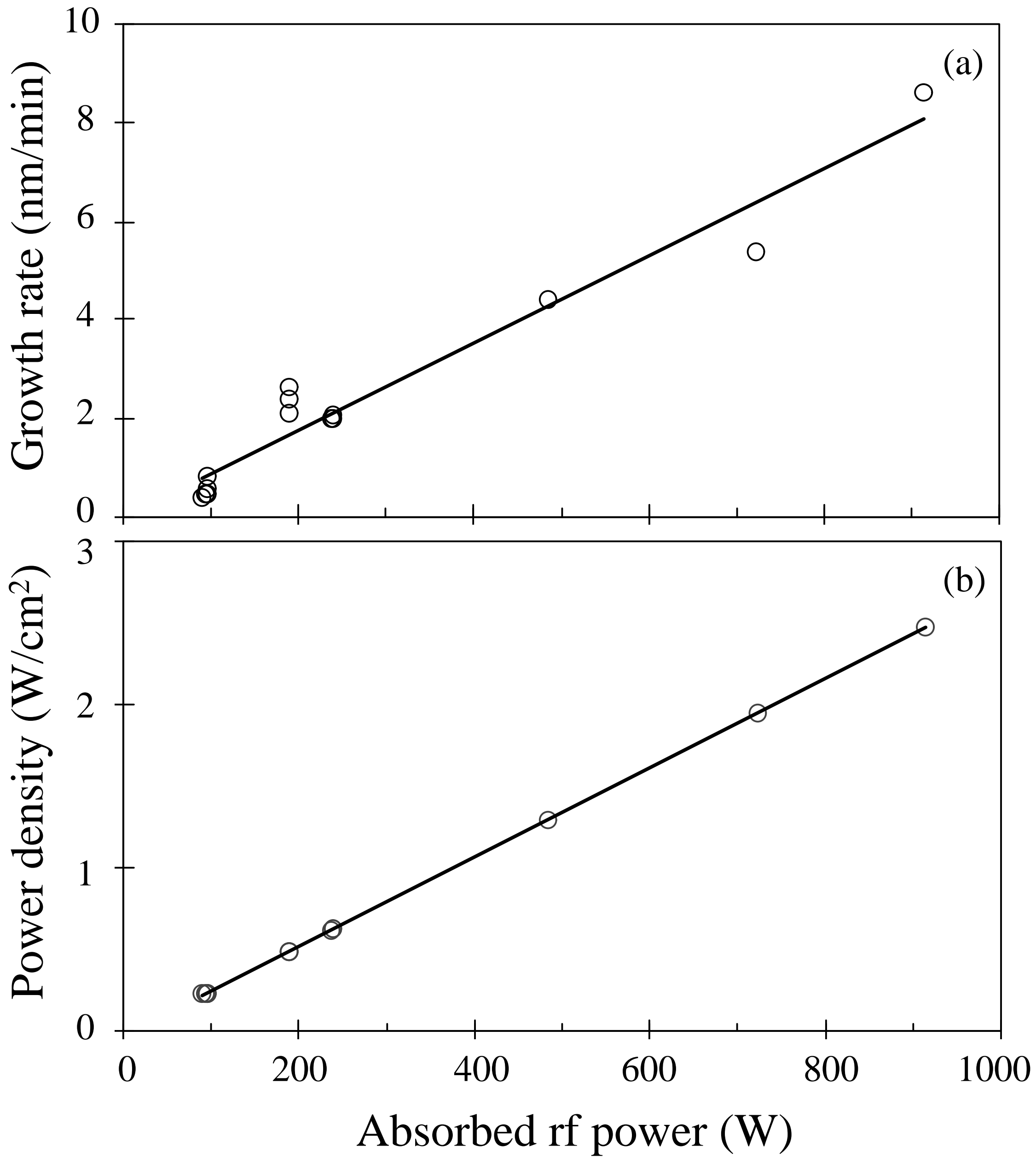

Figure 5

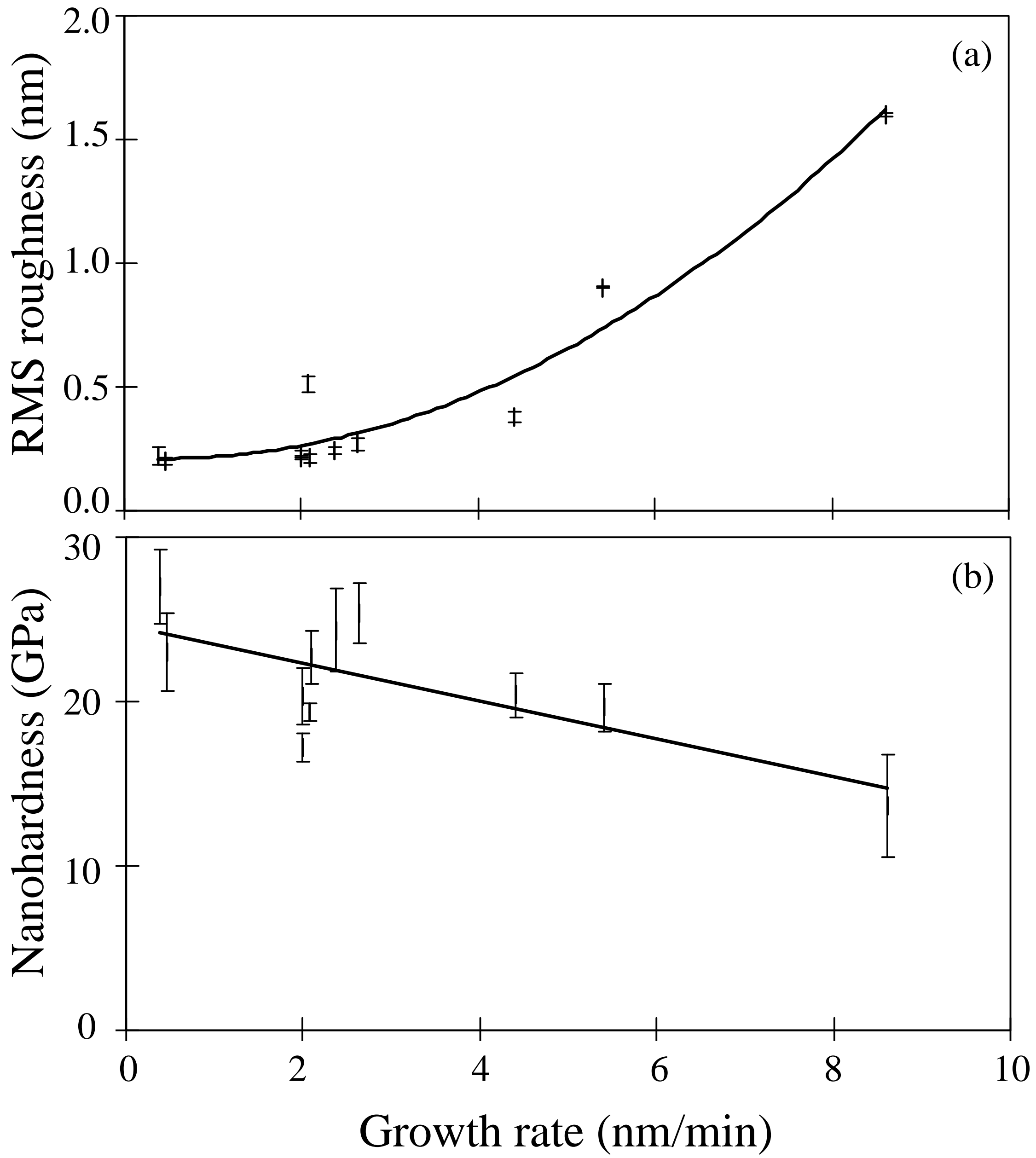

Figure 6

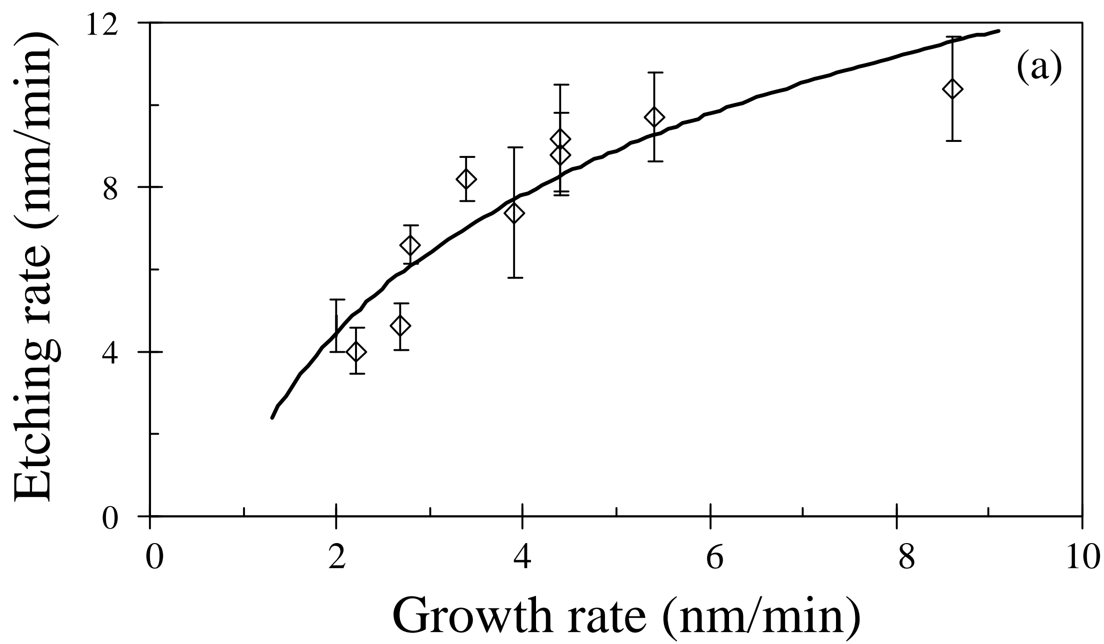

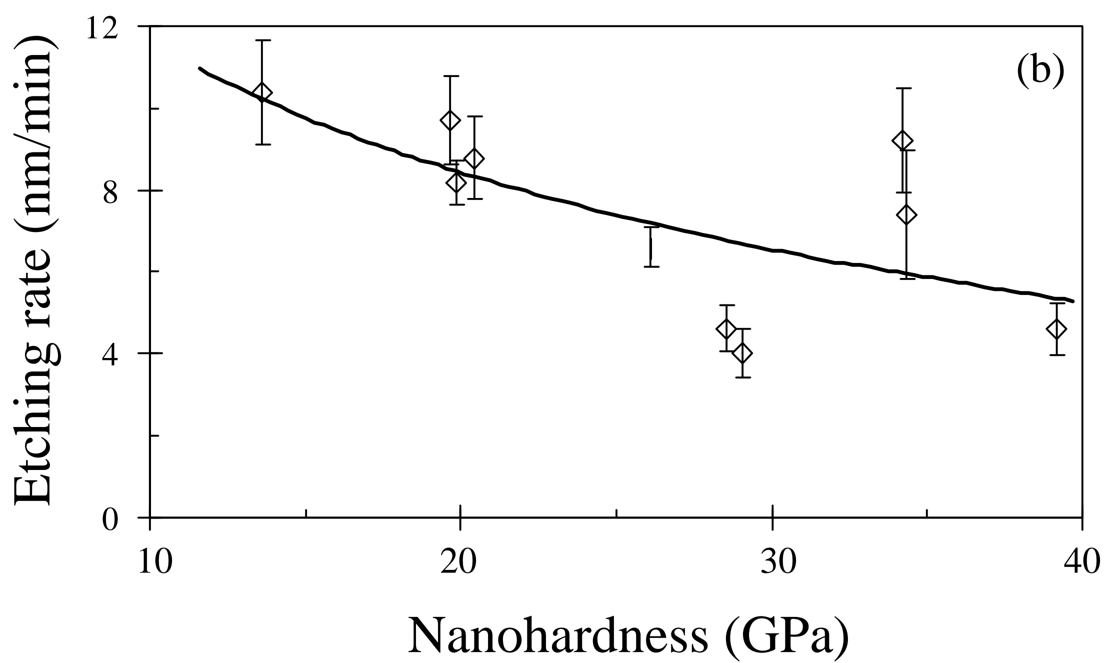

Figure 7

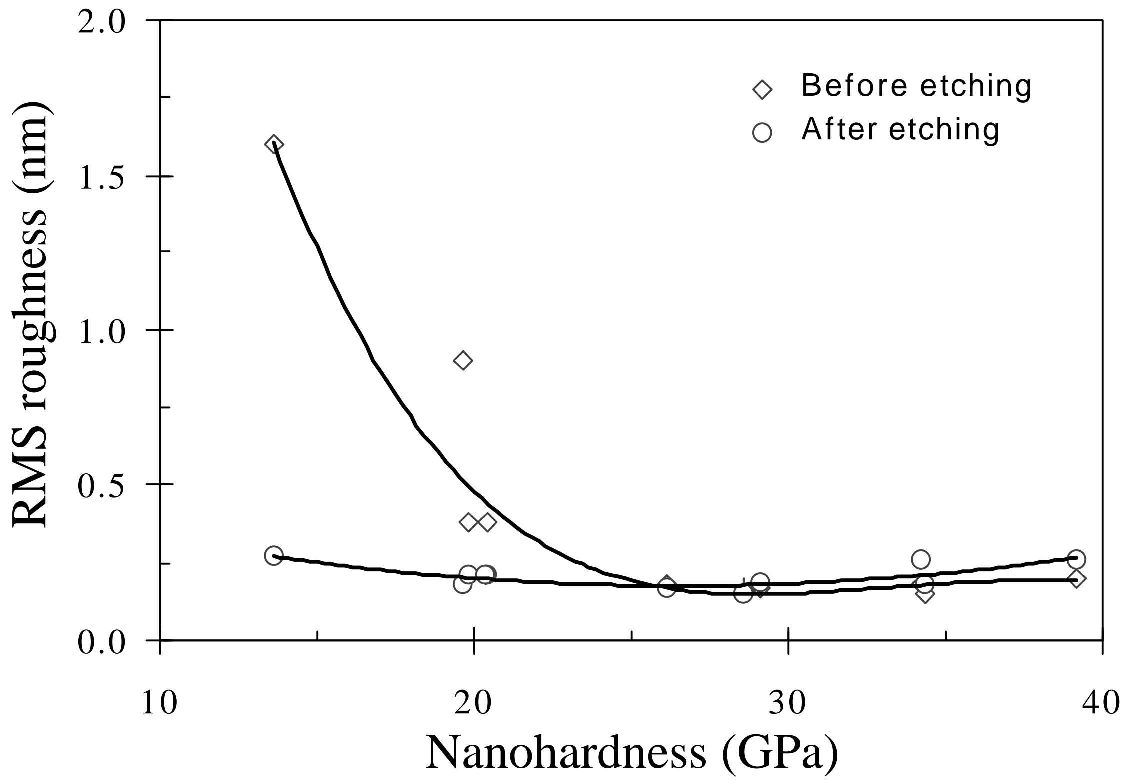

Figure 8

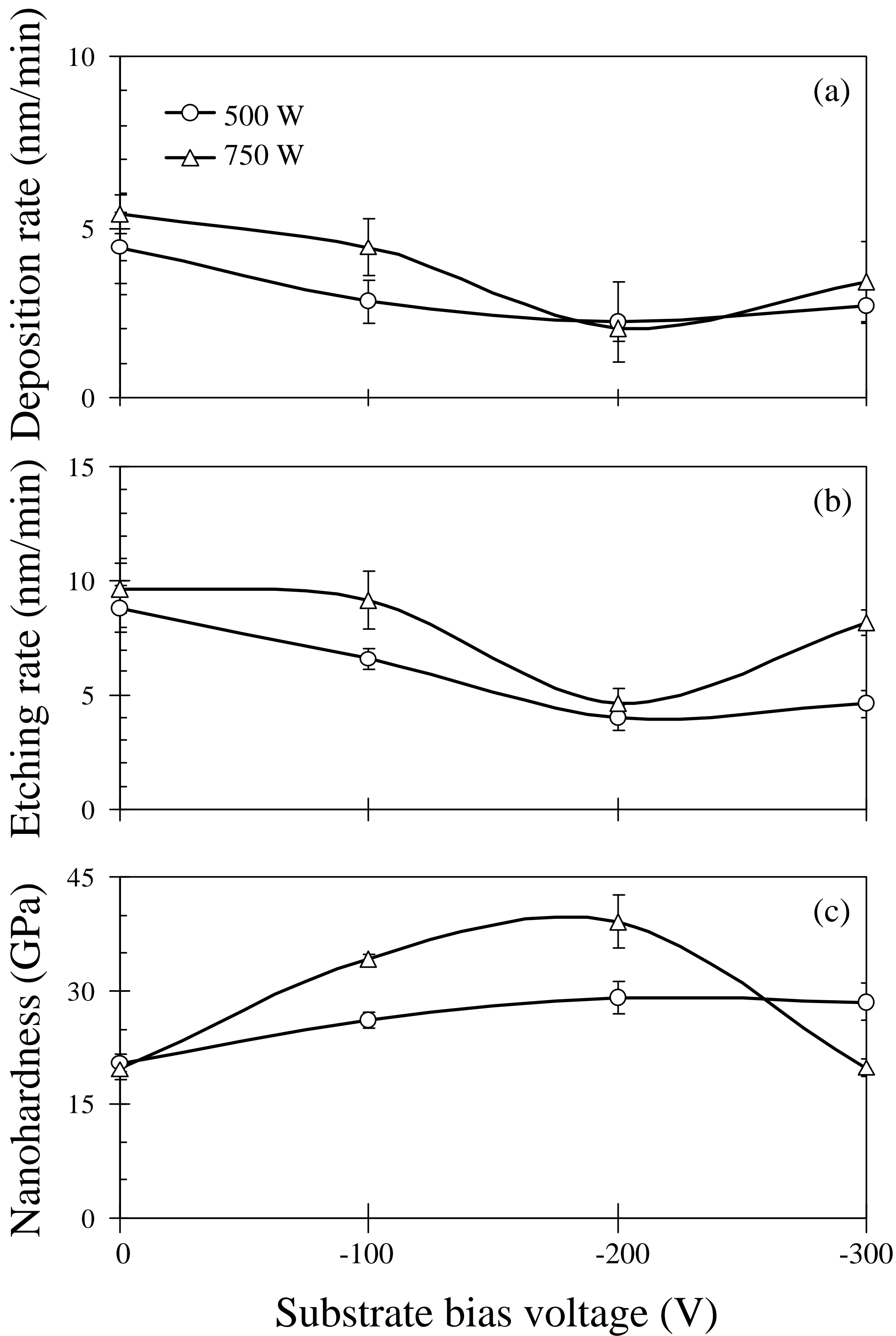

Figure 9

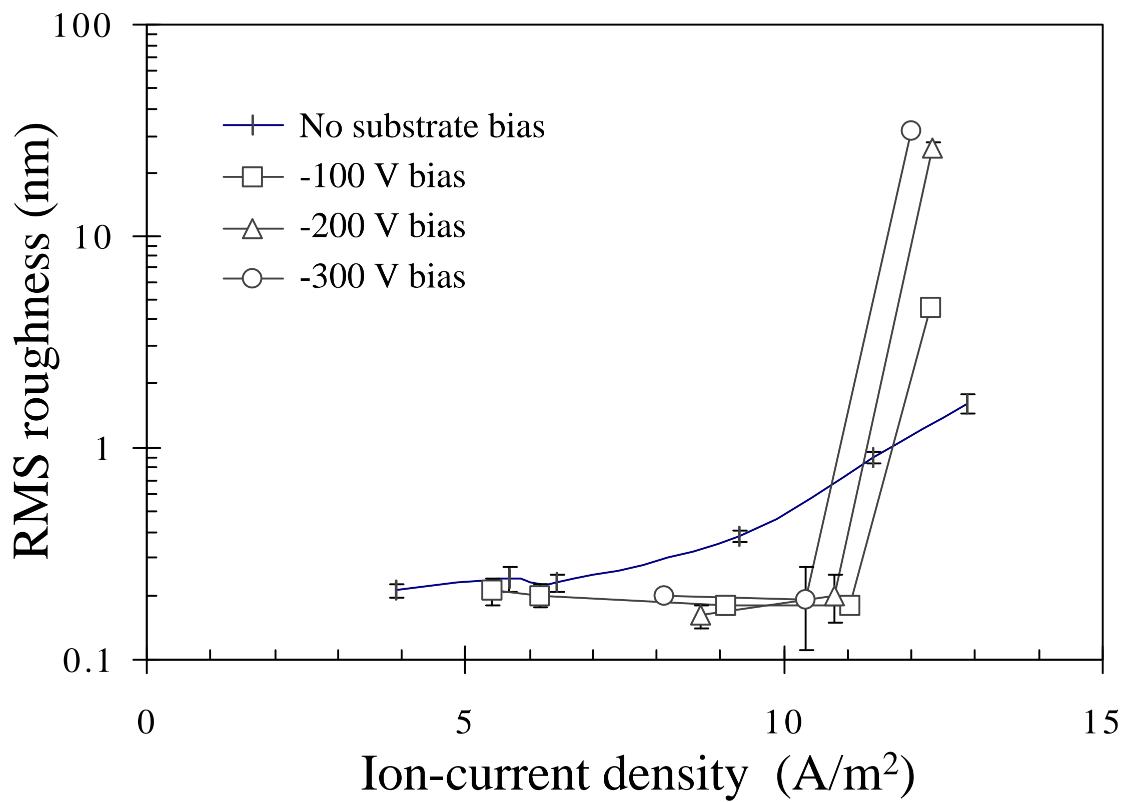

Figure 10

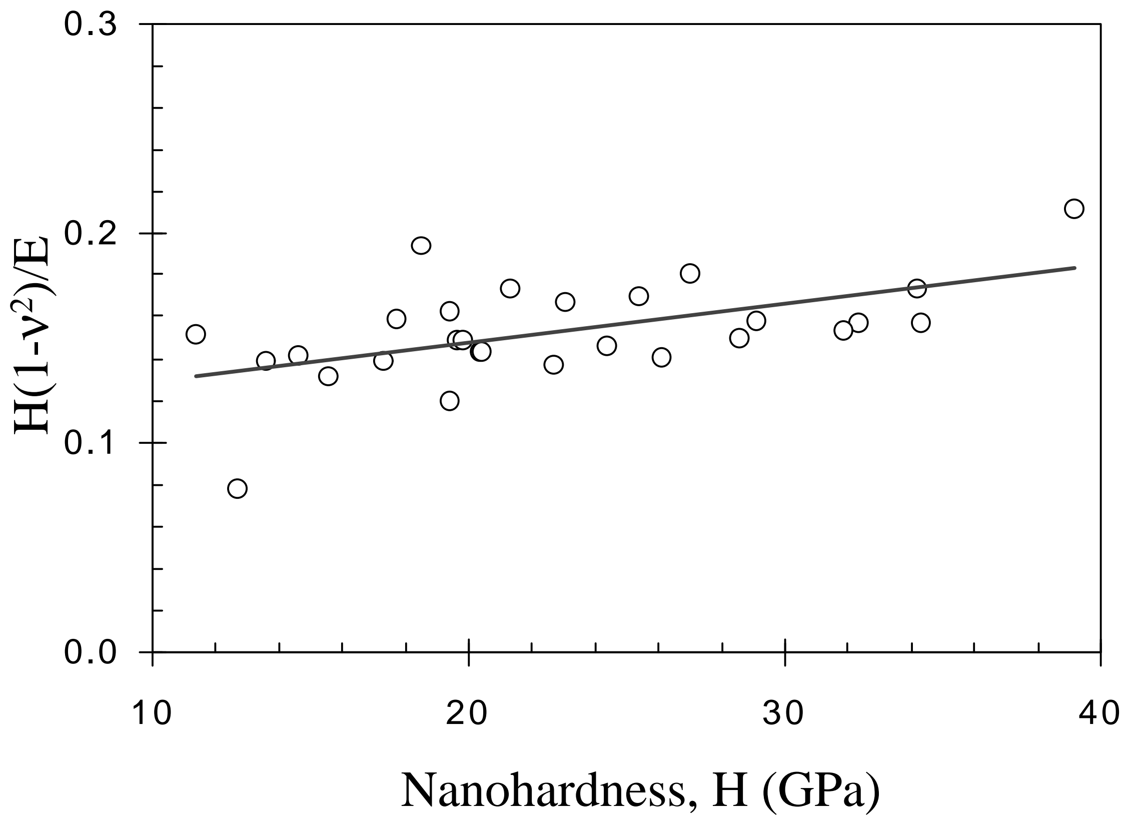

Figure 11

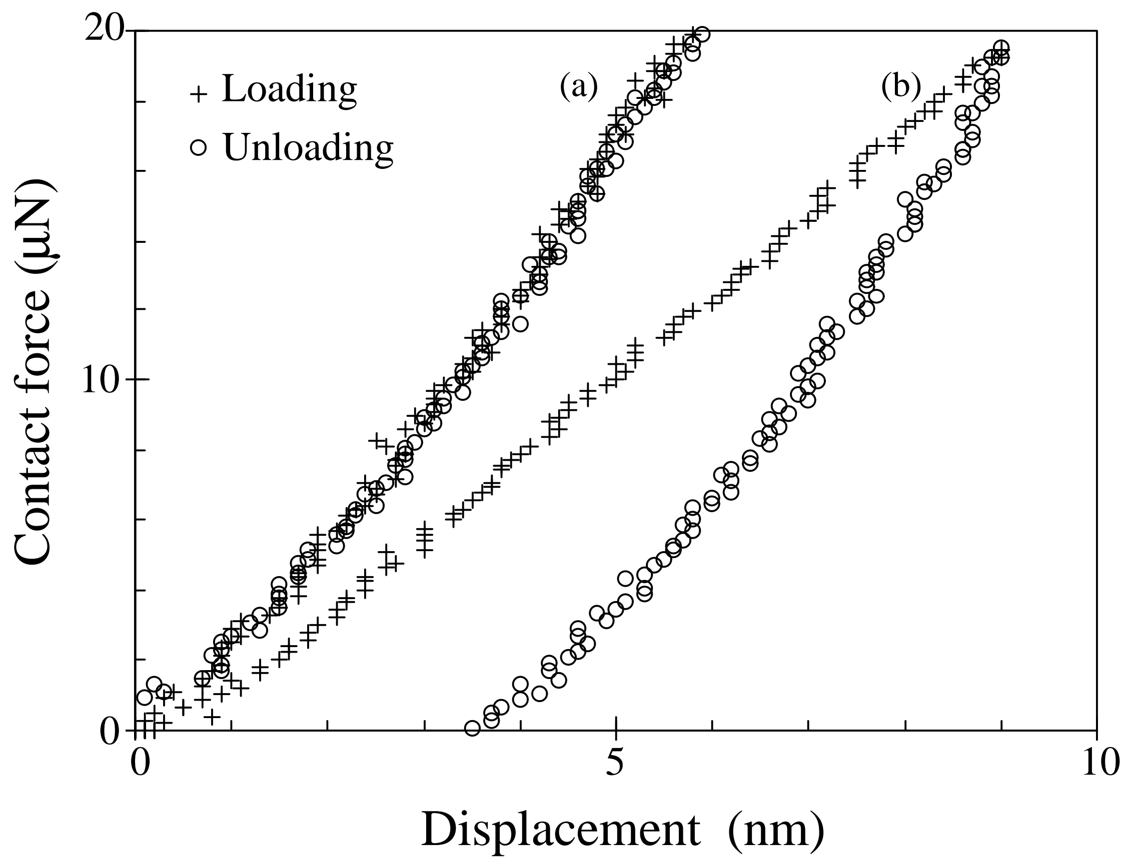

Figure 12

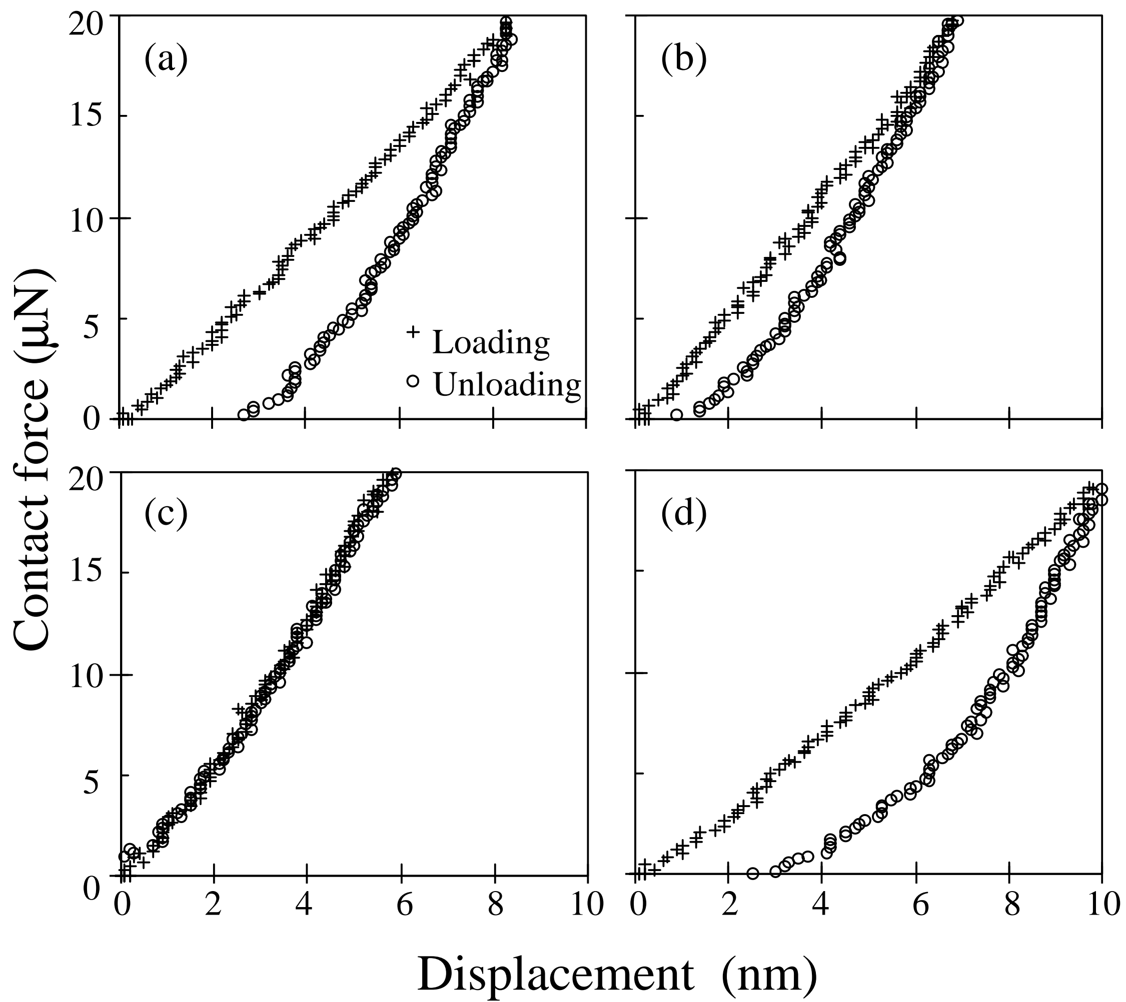

Figure 13

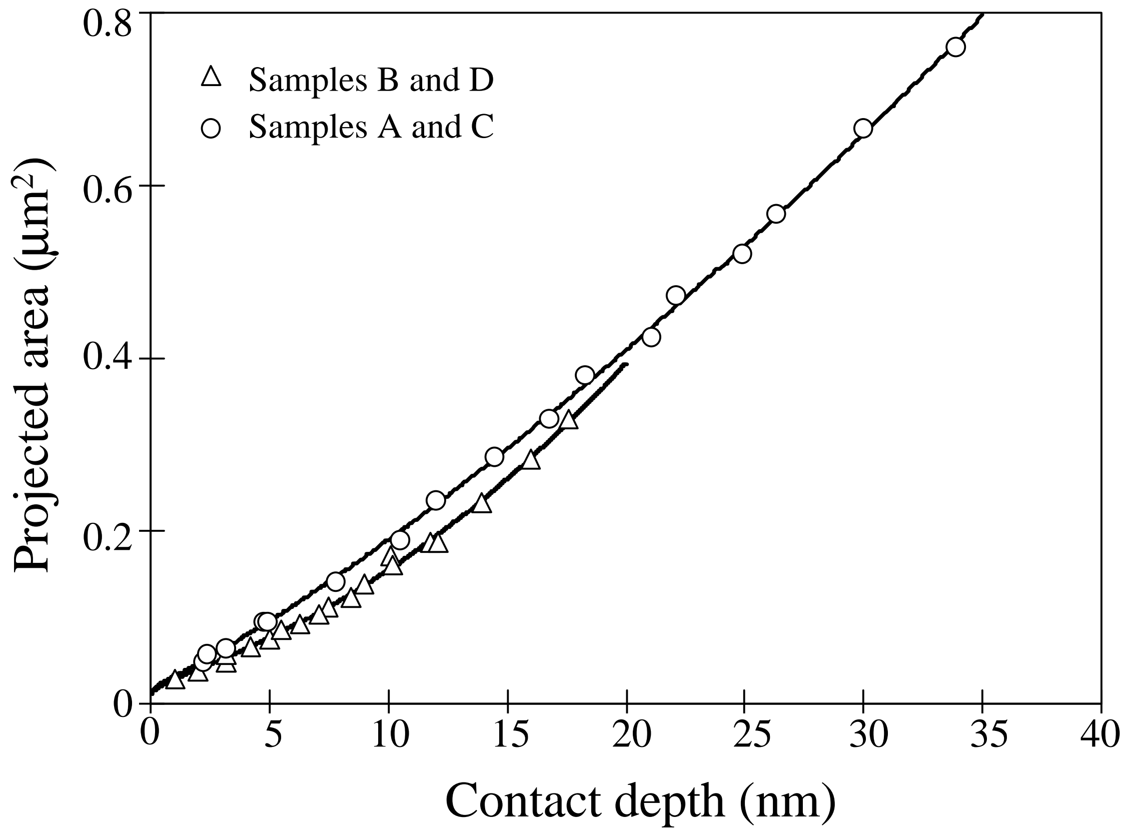

Figure 14